Integrin-mediated targeting of drug delivery to irradiated tumor blood vessels

Dennis Hallahan,[1,3,4,5,*] Ling Geng,[1] Shimian Qu,[1] Christopher Scarfone,[1,2]
Todd Giorgio,[3] Edwin Donnelly,[2] Xiang Gao,[1] and Jeff Clanton[2]

[1]Department of Radiation Oncology
[2]Department of Radiology
[3]Department of Biomedical Engineering
[4]Department of Cancer Biology
[5]Vanderbilt-Ingram Cancer Center
Vanderbilt University, Nashville, Tennessee 37232
*Correspondence: dennis.hallahan@mcmail.vanderbilt.edu

Summary

The objective of this study was to target drug delivery to radiation-induced neoantigens, which include activated receptors within the tumor vasculature. These responses include posttranslational changes in pre-existing proteins, which can be discovered by phage-displayed peptide libraries administered to mice bearing irradiated tumors. Phage-displayed peptides recovered from irradiated tumors included the amino acid sequence RGDGSSV. This peptide binds to integrins within the tumor microvasculature. Immunohistochemical staining of irradiated tumors showed accumulation of fibrinogen receptor $\alpha_{2b}\beta_3$ integrin. We studied tumor targeting efficiency of ligands to radiation-induced $\alpha_{2b}\beta_3$. Radiopharmaceuticals were localized to irradiated tumors by use of $\alpha_{2b}\beta_3$ ligands conjugated to nanoparticles and liposomes. Fibrinogen-conjugated nanoparticles bind to the radiation-activated receptor, obliterate tumor blood flow, and significantly increase regression and growth delay in irradiated tumors. Radiation-guided drug delivery to tumor blood vessels is a novel paradigm for targeted drug delivery.

Introduction

Tumor-specific drug delivery has the potential to minimize toxicity to normal tissues and improve bioavailability of cytotoxic agents to neoplasms (Arap et al., 1998; Hallahan et al., 1995a; Kasahara et al., 1994). Existing site-specific drug delivery systems include adenovirus-targeted delivery to endothelial receptor $\alpha_v\beta_3$ (Brooks et al., 1994; Wickham et al., 1995), and tumor-specific antigens (Ito et al., 1991; Kirpotin, 1997; Manome et al., 1994). Antibody conjugation to cytotoxic agents has shown promise in achieving the goal of tumor-targeted cytotoxicity (Hellstrom et al., 1996; Pastan, 1997). This approach may be limited by the small subsets of tumors that can be targeted by these antibodies and by poor biodistribution of antibodies into solid tumors (Dvorak et al., 1991; Jain, 1997; Shockley et al., 1991). Alternative approaches to target all neoplasms exploit integrins and antigens on proliferating microvasculature (Arap et al., 1998; Baillie et al., 1995; Brooks et al., 1994; Burg et al., 1999; Ellerby et al., 1999; Fox and Harris, 1997; Molema et al., 1997; Pasqualini and Ruoslahti, 1996; Hood et al., 2002). Inducible antigens include proteins in the microvasculature of irradiated tumors, which are antigenic targets for site-specific drug delivery to tumor blood vessels (Hallahan et al., 1995b, 1996, 1998). We studied the tumor-targeting efficiency of phage peptide libraries that bind to radiation-induced proteins.

Studies of irradiated tumor microvasculature have identified receptors and adhesion molecules that contribute to the biological response to therapy (Hallahan et al., 1998, 1999). Although changes in protein expression can be measured, posttranslational modification of integrins, receptors, and adhesion molecules might best be detected by use of phage display peptide libraries (Arap et al., 1998; Forrer et al., 1999; Rajotte and Ruoslahti, 1999). We utilized phage peptide libraries to (Zwick et al., 1998) discover radiation-activated receptors. Peptide binding has been well characterized for ligand interaction with integrins. Among the most prevalent sequence motifs is the amino acid

SIGNIFICANCE

Targeted drug delivery is achieved by use of antibodies that bind selectively to tumor antigens. This strategy of targeted therapy may be limited by the low percentage of neoplasms that express any given antigen. Alternatively, neoantigens are induced within neoplasms following treatment with ionizing radiation. To increase the spectrum of antigenic targets for drug delivery, radiation-induced neoantigens within tumor microvasculature were targeted for drug delivery. Here we show that ligand binding to radiation-activated receptors achieves site-specific drug delivery to irradiated tumor microvasculature. The biologic effect of this targeting strategy is obliteration of tumor blood flow by ligand-conjugated nanoparticles. Obliteration of tumor microcirculation significantly enhances tumor regression and growth delay. This paradigm of site-specific drug delivery compliments existing forms of targeted drug delivery.

sequence arginine-glycine-aspartic acid, RGD, which is a major recognition system for cell adhesion and binds to approximately half of the known integrins. Integrins are heterodimeric proteins in which each of the subunits contributes to ligand specificity and contains binding sites for the ligand. The β3 chain of integrins αvβ3 and α2bβ3 becomes crosslinked to the RGD peptide on the ligand (Smith and Cheresh, 1988). During RGD crosslinking of α2bβ3, RGD binds to the β subunit while the KQAGDV sequence motif binds primarily to the α subunit (Santoro and Lawing, 1987). We utilized the native α2bβ3 ligand, fibrinogen, to achieve targeted drug delivery of radiopharmaceuticals and liposomes to irradiated tumor microvasculature.

Tumor blood vessels have been shown to be a therapeutic target in the treatment of neoplastic diseases (Folkman, 1995). Angiolytic therapy differs from angiostatic therapy in that existing tumor blood flow is destroyed as opposed to the prevention of neovascular development, which results from antiangiogenics. In the present study, obliteration of tumor blood flow was achieved by targeting drug delivery to radiation-activated receptor within tumor blood vessels. Destruction of blood flow was achieved by use of nanospheres, which are particles that contain pharmaceuticals and are designed to embolize tumor microvasculature (McGinity and O'Donnell, 1997). A common nanoparticle core is albumin, which can be loaded with drugs that will be released for prolonged periods of time. Vascular administration of nanoparticles has been designed to localize therapy to tumor blood vessels (Llovet). For example, antibodies have been linked to microspheres to achieve site specificity. We conjugated albumin nanoparticles to ligand that binds to radiation-activated receptor. This approach achieved obliteration of tumor microvascular blood flow and significant enhancement of tumor regression and tumor growth delay.

Results

Peptides recovered from irradiated tumors

The primary objective of this study was to identify receptors and/or cell adhesion molecules in tumor vasculature that are activated or induced by irradiation. These physiologic responses of pre-existing proteins include conformational changes and transport of sequestered proteins, which cannot be detected by use of differential screening of tumors. To identify candidate peptides that bind within irradiated tumor microvasculature, the phage peptide library was injected by tail vein into mice bearing irradiated GL261 and LLC tumors. Phage were recovered from tumors and sequentially re-administered to six mice bearing irradiated tumors. Fifty bacterial colonies were selected from each of two distinct tumor types. Of the peptides recovered from each of the two distinct irradiated tumors, 22% had peptide sequence RGDGSSV. We compared this recombinant phage to wild-type phage for binding within irradiated tumors. The frequency of recovery of the RGDGSSV phage irradiated tumors was compared to that of untreated tumors in the same mice. Of the 10^6 RGDGSSV phage injected, 31 $\pm$ 9 were recovered from irradiated tumors as compared to 0 of 10^6 wild-type and 0 of 10^6 random sequence phage ($p < 0.001$).

Radiation-induced accumulation of α2bβ3 integrin within tumor blood vessels

The RGD sequence within the RGDGSSV peptide has the greatest number of matches in Blast and Swisspro searches. Putative receptors that bind the RGD peptide include the β1, β3, and β5 chains, which heterodimerize with the αv chain to form the $\alpha_v\beta_3$ integrin on the endothelium or with the α2b chain on platelets (Ruoslahti, 1996). To determine whether the level of these integrins increases in response to irradiation, immunohistochemical staining and Western immunoblots were used to study integrins in irradiated tumors. Microscopic photographs of tumor sections are shown in Figure 1. Immunohistochemical staining for integrin $\alpha_{2b}\beta_3$, and the αv chain of integrin $\alpha_v\beta_3$, revealed increased levels of the β_3 chain (Figure 1B) and the α_{2b} chain (Figure 1D) within the lumen of the microvasculature of tumors isolated 6 hr after irradiation, but no increase in untreated control tumors (Figures 1A and 1C). Conversely, staining for the αv chain did not increase after irradiation (Figures 1E and 1F). To determine whether α_{2b} and β_3 chain staining correlated with platelet accumulation, tumor sections were stained for P-selectin. This showed P-selectin staining in the endothelium prior to irradiation, and P-selectin accumulation in the lumen of tumor blood vessels after irradiation (Figures 1G and 1H). To verify that α2bβ3 accumulates within irradiated tumor blood vessels, Western immunoblot using anti-α2b antibody was performed. Protein extracted from tumors shown in Figures 1C and 1D was separated by SDS-PAGE. Figure 1I shows increased α2b chain of the $\alpha_{2b}\beta_3$ integrin beginning at 3 hr and persisting at 6 hr after tumor irradiation.

Ligand binding to receptor in irradiated tumor vasculature

Possible sites of RGDGSSV peptide binding include receptors in the vascular lumen or vascular wall. To determine the pattern of RGDGSSV peptide binding within irradiated tumor blood vessels, we utilized the dorsal skin fold tumor vascular window (Geng et al., 2001). LLC tumors were implanted into intravital windows on C57BL6 mice. FITC-labeled peptide was administered by tail vein injection and tumors were irradiated with 6 Gy. Figure 2 shows fluorescent microscopic photographs obtained at 6 hr after irradiation. Irradiated tumors showed RGDGSSV peptide binding within the lumen of microscopic blood vessels (Figure 2C). Control scrambled peptide was used to determine whether radiation-induced peptide binding was nonspecific. Control peptide showed no increase in binding and blood vessels in unirradiated tumors showed no increase in RGDGSSV peptide binding.

Platelet activation could account for RGDGSSV peptide binding in irradiated tumors. Fibrinogen has two RGD peptides on the α chain, which participate in binding to activated α2bβ3 receptor on platelets. To determine whether fibrinogen binds within blood vessels of mice bearing both irradiated and control tumors, we administered biotinylated fibrinogen by tail vein injection. Fluorescent microscopy of FITC-conjugated avidin staining of biotinylated fibrinogen showed fibrinogen accumulation throughout the lumen of irradiated tumor (Figure 2E) as compared to the patchy staining in untreated control tumor (Figure 2D). To determine whether the biotinylated fibrinogen colocalizes with the α2b chain of $\alpha_{2b}\beta_3$, LLC tumor sections were stained with Cy5-labled antibody for anti-α2b antibody and Cy3-labeled avidin. Figure 2F shows that fibrinogen (green) colocalizes (yellow) with α2b (red) within the tumor vascular lumen. The fibrinogen receptor, integrin α2bβ3, is therefore a candidate radiation-inducible receptor for site-specific drug delivery.

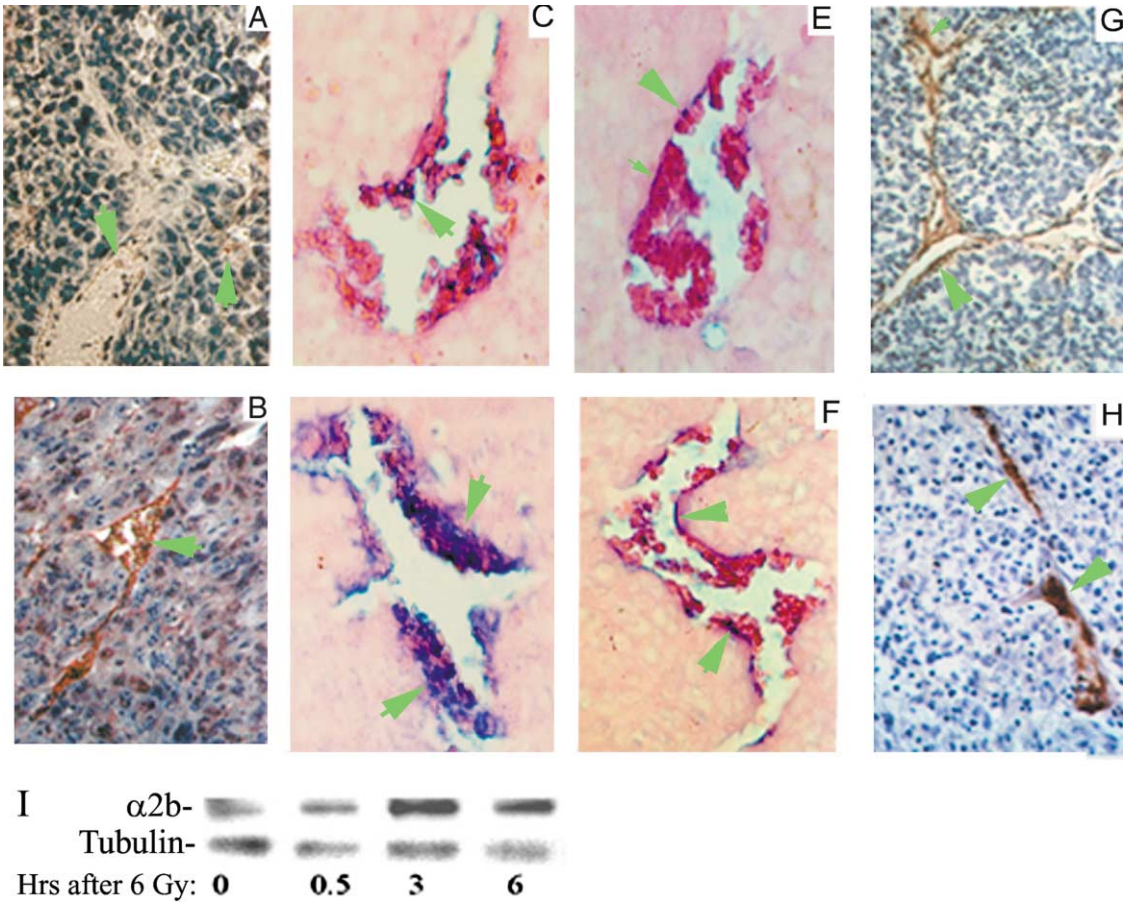

Figure 1. Radiation-induced platelet aggregation in tumor microvasculature

GL261 murine gliomas were implanted into the hind limb of C57BL6 mice. Tumors were grown to a diameter of 10–12 mm over 8–10 days, followed by irradiation. Six hours after irradiation, tumors were dissected and fixed. Shown is immunohistochemical staining for β3 chain (**A** and **B**); the α2b chain (**C** and **D**) of integrin $\alpha_{2b}\beta_3$; and the av chain (**E** and **F**); and P-selectin (**G** and **H**). Shown are tumor sections obtained 6 hr after 0 Gy (upper panels), or 6 hr after 6 Gy (lower panels). Arrows indicate area of positive staining.

I: Protein extracted from tumors shown in **E** and **F** was separated by SDS-PAGE. Shown is the autoradiograph from Western Immunoblot using antibody to the α2b chain of integrin $\alpha_{2b}\beta_3$.

Drug delivery systems targeted to radiation-induced receptor

Drug delivery vehicles such as liposomes and nanoparticles can be conjugated to fibrinogen to accomplish site-specific binding to irradiated tumor blood vessels. Nanoparticles designed to embolize tumor microvasculature include albumin within the core, which can be radiolabeled with internal emitters for imaging (Martodam et al., 1979; McGinity and O'Donnell, 1997; Saltzman and Fung, 1997). To determine whether integrin $\alpha_{2b}\beta_3$ can serve as a target for imaging, fibrinogen-conjugated nanoparticles were radiolabeled. Nanoparticles consisting of an albumin aggregate core, coated with fibrinogen (Fbg-NP), were radiolabeled with ^{131}I and administered by tail vein injection into tumor bearing mice (Figure 3). GL261 glioma and B16F0 melanoma tumors were implanted into C57BL6 mice and irradiated with 6 Gy. Specificity of Fbg-NP was determined by well counts of tumor and other tissues. Figure 3 shows that 91% of counts were localized to tumors while 9% were diffusely distributed throughout the entire animal model as compared to untreated controls, which showed 10% of counts in tumor ($p < 0.001$).

During optimization studies, tumors were irradiated immediately before or immediately after tail vein injection. Both schedules were effective in achieving ^{131}I-fibrinogen-coated nanoparticle binding. However, tumor irradiation after nanoparticle administration achieved increased specificity of radiolabeled protein binding as compared to tumors irradiated prior to administration (Figure 3B). This finding could be explained by native unlabeled fibrinogen in the circulation competing for activated $\alpha_{2b}\beta_3$ before the administration of Fbg-NP. Albumin nanoparticles without fibrinogen conjugation were used as negative controls. Control nanoparticles were radiolabeled with ^{131}I and administered by tail vein to mice bearing irradiated B16F0 tumors. Figure 3C shows that nanoparticles do not bind in irradiated tumors unless they are coated with fibrinogen. To compare tumor-specific binding of radiolabeled albumin nanoparticles to that of radiolabeled Fbg-NP, we removed tumors and measured tissue weight and well counts of tumor and whole body. The ratio of (CPM tumor/weight tumor) to (CPM whole body/weight whole body) showed 102-fold tumor specificity for Fbg-NP. In comparison, radiolabeled albumin nanoparticles showed no

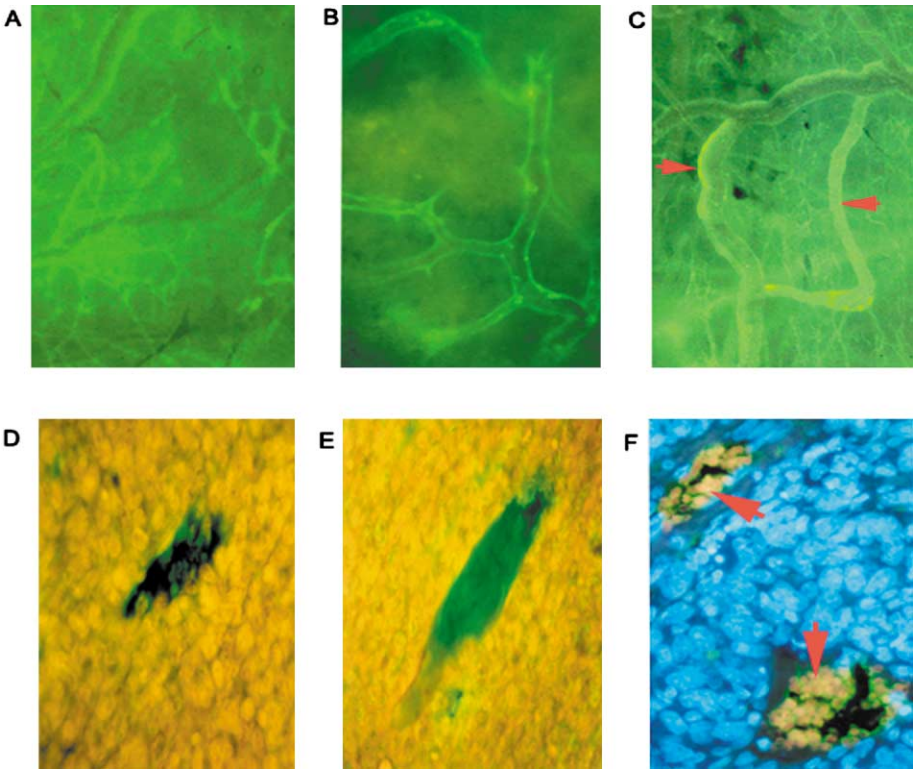

Figure 2. Peptide binding within intravital tumor vascular window

LLC tumors were implanted into dorsal skin fold windows of C57BL6 mice. Tumors were irradiated and FITC-labeled peptide was administered. Shown are fluorescent microscopic photographs obtained at 6 hr after (**A**) irradiation and "scrambled" control peptide, (**B**) RGDGSSV peptide and 0 Gy, (**C**) RGDGSSV peptide and 6 Gy. Arrows indicate FITC-labeled peptide accumulation within vasculature.

D and **E:** Biotinylated fibrinogen binding in irradiated tumor blood vessels is shown. Tumors were implanted into both hind limbs of mice. The right tumor was irradiated and the left served as an untreated internal negative control. Biotinylated fibrinogen was administered by tail vein injection immediately prior to tumor irradiation. Shown are fluorescent microscopic photographs of (**D**) control and (**E**) irradiated tumors.

F: Colocalization of Fbg-NP with antibody to α2b. Fbg-NP were biotinylated and injected by tail vein into LLC tumor bearing mice. Tumors were immediately irradiated using 6 Gy while shielding the body of the mouse. Shown are microscopic (100×) photographs of tumor sections stained with avidin and anti-α2b antibody. Arrow indicates nanoparticle and α2b co-staining.

increase in binding to irradiated tumor as compared to all other normal tissues (Figure 3C).

A potential limitation in the use of fibrinogen to target drug delivery is the risk of thromboembolic events in vital organs. To determine whether fibrinogen-coated nanoparticles bind within specific organs, we measured ^{131}I in organs by use of well counts and studied nanopartcle binding by microscopy. Figure 3D shows ^{131}I labeled nanoparticles quantified by well counts of the lungs, kidneys, livers, spleens, and hind limbs of each of the mice. The bar graph shows counts from each of these organs comparing ^{131}I -nanoparticle alone to ^{131}I-Fbg-NP. Tumors trap 91% of Fbg-NP following irradiation, and the remaining 9% binds primarily in the spleen (4.4%). The remaining 4.6% was distributed equally throughout the entire blood volume, with less than 1% in lung, liver, kidney, and hind limb, respectively. There was no increase in Fbg-NP binding within the irradiated hind limb as compared to untreated controls. Likewise, unirradiated lungs, kidneys, and livers showed no increase in Fbg-NP binding. Conversely, the spleen showed increased Fbg-NP binding as compared to uncoated nanoparticle controls (Figure 3D). Organs from mice shown in the bar graph were sectioned and stained for biotinylated nanoparticles. Shown are representative microscopic photographs of biotinylated Fbg-NP in lung and spleen. Fbg-NP were trapped within irradiated tumors and little binding occurred within the spleens, and there was no increase in binding within blood vessels of other organs.

Diminished binding in regions of low blood flow in tumors is a second potential limitation of targeted drug delivery. To determine the biodistribution of Fbg-NP within irradiated tumors, Fuji plate imaging of ^{131}I-labeld Fbg-NP microdosimetry was performed. Blood flow in GL261, LLC, and B16F0 tumors was imaged by Doppler blood flow (Geng et al., 2001) prior to the administration of radiolabeled Fbg-NP. Figure 4 shows blood flow primarily in the periphery of all tumors and less flow within the center of tumors. In comparison, the pattern of γ emission from ^{131}I-labeld Fbg-NP is shown in the lower panels of Figure 4. Gamma emission from tumor sections at 6 hr after treatment shows that radiolabeled particles are distributed throughout the tumor sections, and are primarily localized to areas of higher blood flow. The distribution of γ emission from nanoparticles in tumor sections correlated well with the corresponding patterns of blood flow imaged by Doppler.

Liposome conjugates are an alternative drug delivery vehicle to nanoparticles. For example, antibody-liposome conjugates have been used to target drug delivery to tumor blood vessels (Boerman et al., 2001; Sipkins et al., 2000). We conjugated fibrinogen to long circulating liposomes. Liposomes were labeled with the fluorescent marker DiI and administered by tail vein into mice bearing tumors on both hind limbs. The right tumor was treated with radiation and the left tumor served as the untreated internal control. Untreated control tumors showed no fibrinogen-liposome conjugate binding (Figure 5A) whereas tumors irradiated immediately before or immediately after tail vein injection showed fibrinogen-liposome in blood vessels (Figure 5B). The fluorescent marker was found within the vascular lumen of tumor microvasculature. We studied the tumor-targeting potential by radiolabeling the fibrinogen-liposome conjugates. Figure 5C shows that 89% of radiolabeled liposome conjugates were localized to tumors treated with radiation after administration of liposomes as compared to 9% in untreated tumors (0 Gy) ($p < 0.001$), while 75% of radiolabeled liposome conjugates were localized in tumors treated immediately after injection.

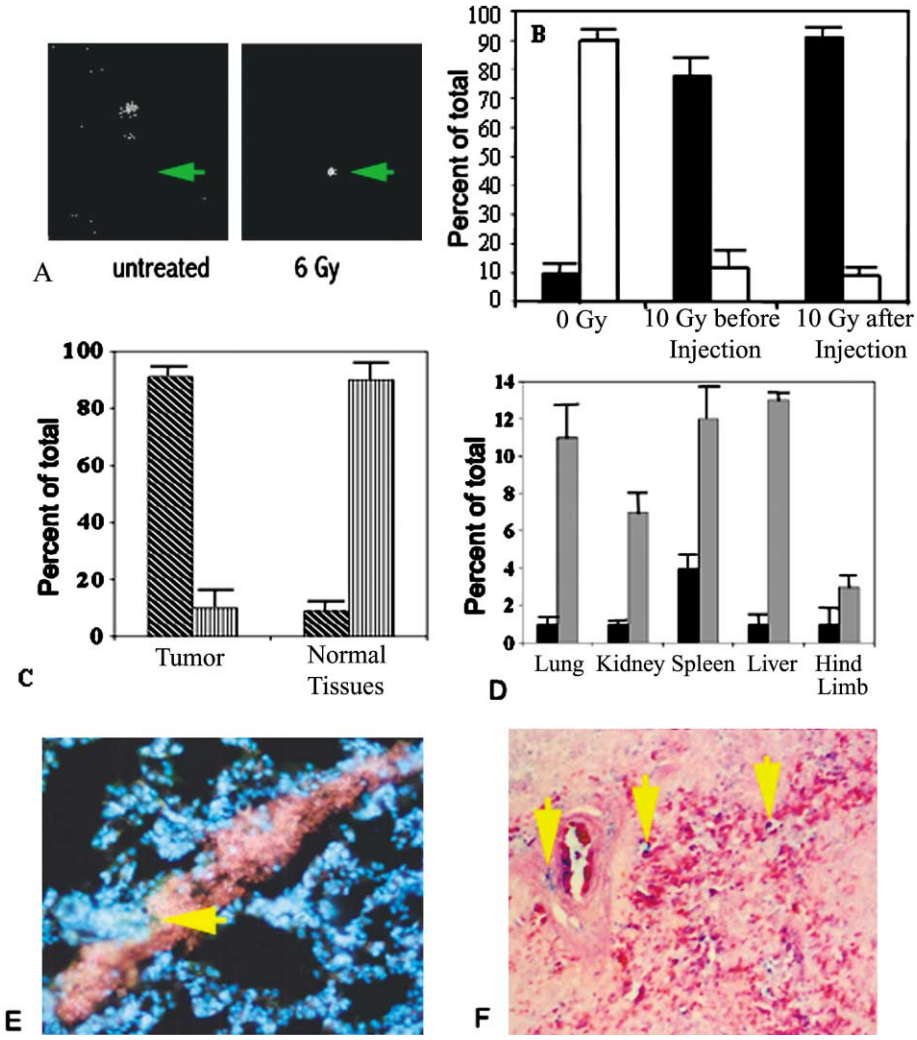

Figure 3. Fbg-NP were radioiodinated by use of iodogen

A: B16F0 murine melanomas were implanted into the hind limbs of C57BL6 mice. ^{131}I-nanoparticles were administered by tail vein injection and mice were imaged by pinhole collimator on an Anger γ camera. Shown are images representative of scans of mice following tumor irradiation with 0 Gy or 6 Gy after Fbg-NP administration. Arrows show the location of tumor markers that were imaged prior to ^{131}I imaging.

B: Tumors were excised and well counts of tumor and whole animal were measured. Shown are the mean and SEM of well counts of whole body (white bars) and tumor (black bars) from five animals in each group.

C: Albumin nanoparticles serving as negative controls were radiolabeled with ^{131}I and administered by tail vein to mice bearing irradiated tumors. Shown are the mean and SEM of well counts of whole body and tumor from mice injected with Fbg-NP (diagonal stripes) or control albumin nanoparticles (vertical stripes) in five animals in each group.

D: ^{131}I-labeled nanoparticles were quantified by well counts of the lungs, kidneys, livers, spleens, and hind limbs of each of the mice. The bar graph shows percentage of total counts in each organ from mice treated with Fbg-NP and radiation (black bars), or control nanoparticles and radiation (gray bars).

E: Organs from mice shown in Figure 3D were sectioned and stained for biotinylated nanoparticles. Shown are representative microscopic photographs (100×) of staining for nanoparticles in lung and spleen. Yellow arrows indicate stained Fbg-NP.

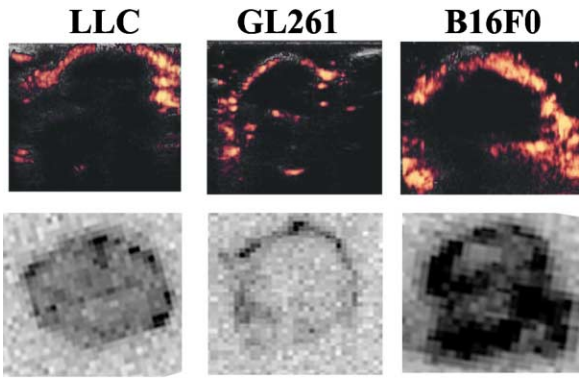

Figure 4. Biodistribution of Fbg-NP within irradiated tumors

Blood flow in LLC, GL261, and B16F0 tumors was imaged by use of Doppler sonography prior to the administration of radiolabeled Fbg-NP (upper panels). Tumors were sectioned 6 hr after the administration of Fbg-NP and placed onto Fuji plates (lower panels). The distribution of Fbg-NP was compared to the pattern of blood flow in these same tumors. Shown are the patterns of γ emission of tumor sections detected by Fuji imaging plates and the corresponding patterns of blood flow imaged by Doppler.

Tumor vascular response to radiation-targeted nanoparticles

An advantage to targeting drug delivery to tumor vasculature is that the blood vessels within neoplasms are effective therapeutic targets. To determine whether nanoparticles targeted to radiation-inducible $\alpha_{2b}\beta 3$ can achieve tumor vascular obstruction, we studied blood flow in treated tumors. Amplitude modulated three-dimensional Doppler sonography (Power Doppler) quantifies tumor microvascular blood flow (Geng et al., 2001). B16F0 hind limb tumors were irradiated and Fbg-NP were administered by tail vein. Tumor blood flow was imaged by use of Power Doppler prior to and 3 days after treatment (Figure 6). Tumors were treated with 10 Gy, 10 Gy with uncoated nanoparticles, 0 Gy, and 10 Gy with Fbg-NP. Sonographic measurement of microscopic blood flow showed that radiation alone or nanoparticle controls achieved minimal change in tumor blood flow. Tail vein administration of Fbg-NP immediately prior to irradiation achieved tumor-specific reduction in tumor blood flow that persisted at 72 hr after irradiation (Figure 6G). Quantification of blood flow showed an 85% reduction in tumors treated with Fbg-NP and radiation as compared to no change in tumors treated with 10 Gy or uncoated nanoparticles with 10 Gy ($p = 0.023$).

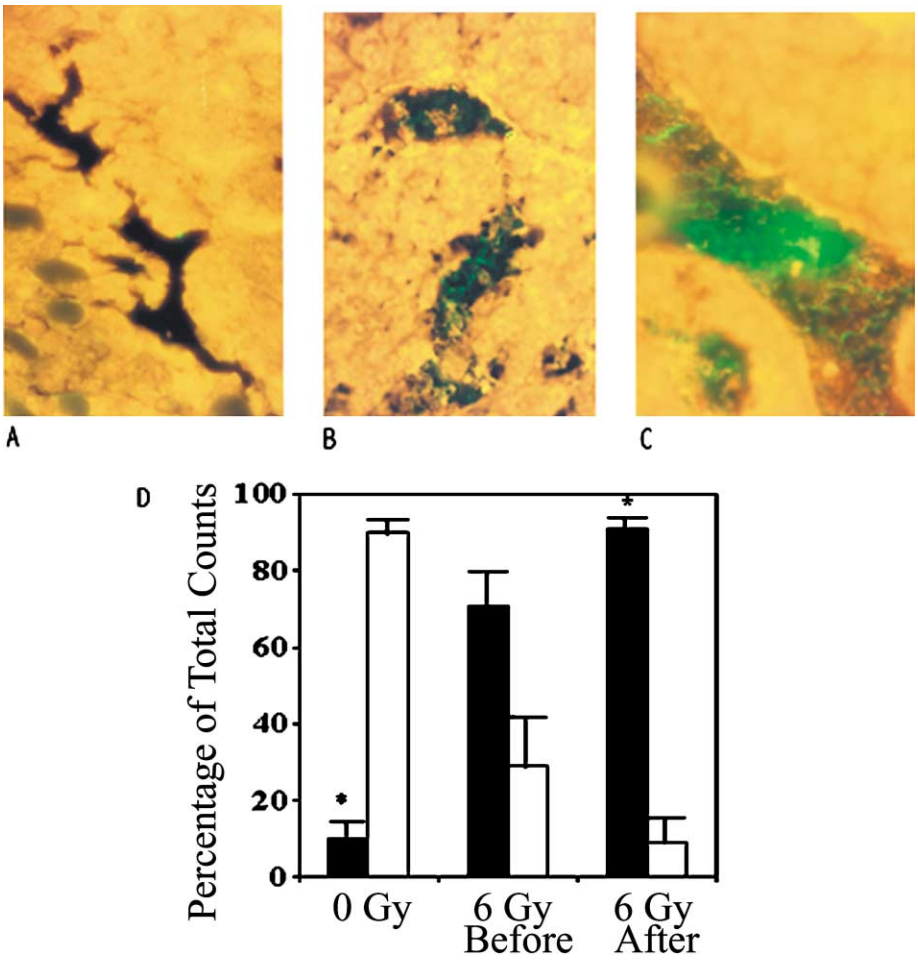

Figure 5. Fibrinogen-liposome conjugates localized to irradiated tumors

Thiolated fibrinogen was conjugated to maleimide containing liposome vesicles. Liposomes were labeled with DiI fluorescent marker and administered by tail vein to tumor bearing mice. Tumors were treated with 4 Gy either prior to administration or after administration of fibrinogen-liposome conjugates. Tumors were fixed and sectioned at 24 hr following irradiation. Shown are tumor sections of (**A**) sham irradiated, (**B**) irradiation prior to fibrinogen-liposome administration, and (**C**) irradiation after fibrinogen-liposome administration. Fluorescence was imaged by UV microscopy (100×).

D: Radiolabeled fibrinogen-conjugated liposomes were administered to mice treated with 0 Gy, 6 Gy before injection, or 6 Gy after injection. Shown are the percentages of well counts from five tumors (black bars) and normal tissues (white bars) after excision of tumors. * Irradiated tumors show significantly increased ^{131}I-Fibrinogen liposome binding as compared to unirradiated tumors ($p < 0.001$).

Tumor vascular thrombosis could be activated by exogenous fibrinogen or binding peptide alone. To determine whether α2bβ3 binding peptide or fibrinogen reduce tumor blood flow when combined with irradiation, these proteins were used as controls. Tumors treated with fibrinogen and 10 Gy, or HHL GGAKQAGDV peptide and 10 Gy, showed no reduction in blood flow (Figure 6G). Fbg-NP are required to obstruct blood flow within tumors. The α2b-blocking antibody was used to determine whether the biological effect required Fbg-NP binding to a2bb3 receptor. Blocking antibody administered immediately prior to Fbg-NP and irradiation significantly attenuated the reduction in blood flow. Tumors treated with antibody showed blood flow that was 90% as compared to blood flow measured prior to irradiation, while Fbg-NP and radiation reduced blood flow to 15% as compared to blood flow at the 0 hr time point ($p = 0.048$).

Disruption of blood flow by nanoparticles could be a nonspecific effect of particle embolization within blood vessels. To determine the mechanism by which radiation and Fbg-NP diminish blood flow, tumor sections were stained for thrombus formation. Figures 6E and 6F show H&E staining of tumors irradiated after tail vein injection of uncoated nanoparticles or Fbg-NP, respectively. Arrows indicate thrombus formation within a treated tumor blood vessel. In comparison, tumors treated with radiation and uncoated nanoparticles or treated with Fbg-NP alone showed no thrombus formation (Figure 6E).

To validate the interaction between radiation and Fbg-NP, the dorsal skin fold windows of LLC tumor blood vessels were imaged by microscopy. Figure 7 shows representative microscopic photographs of tumor vascular windows before (upper panels) and after (lower panels) treatment with uncoated nanoparticles and radiation, Fbg-NP alone, or combined Fbg-NP and radiation. Tumor blood vessels treated with 3 Gy and Fbg-NP were destroyed within 72 hr, whereas radiation and control nanoparticles or Fbg-NP alone produced minimal reduction in tumor blood vessels (Figure 7). The bar graph shows the mean and SEM of five tumors in each of these treatment groups. Tumor blood vessels treated with 3 Gy and Fbg-NP had a mean vascular linear density that was 5% that of the same tumors prior to treatment ($p = 0.015$). In comparison, radiation and control nanoparticles or Fbg-NP alone produced no significant reduction in tumor blood vessels to 91% and 83%, respectively.

Tumor regression and growth delay

Embolization or thrombosis of tumor vasculature can produce tumor regression (Llovet et al., 2002; Hallahan et al., 1995a). To determine whether radiation-induced activation of the fibrinogen receptor is a therapeutic target for vascular embolization, we utilized fibrinogen-coated albumin nanoparticles. Fbg-NP were administered immediately prior to irradiation of tumors. Figure 8 shows fold increase in mean tumor volume as compared to that measured on the day of treatment (Day 1). Fbg-

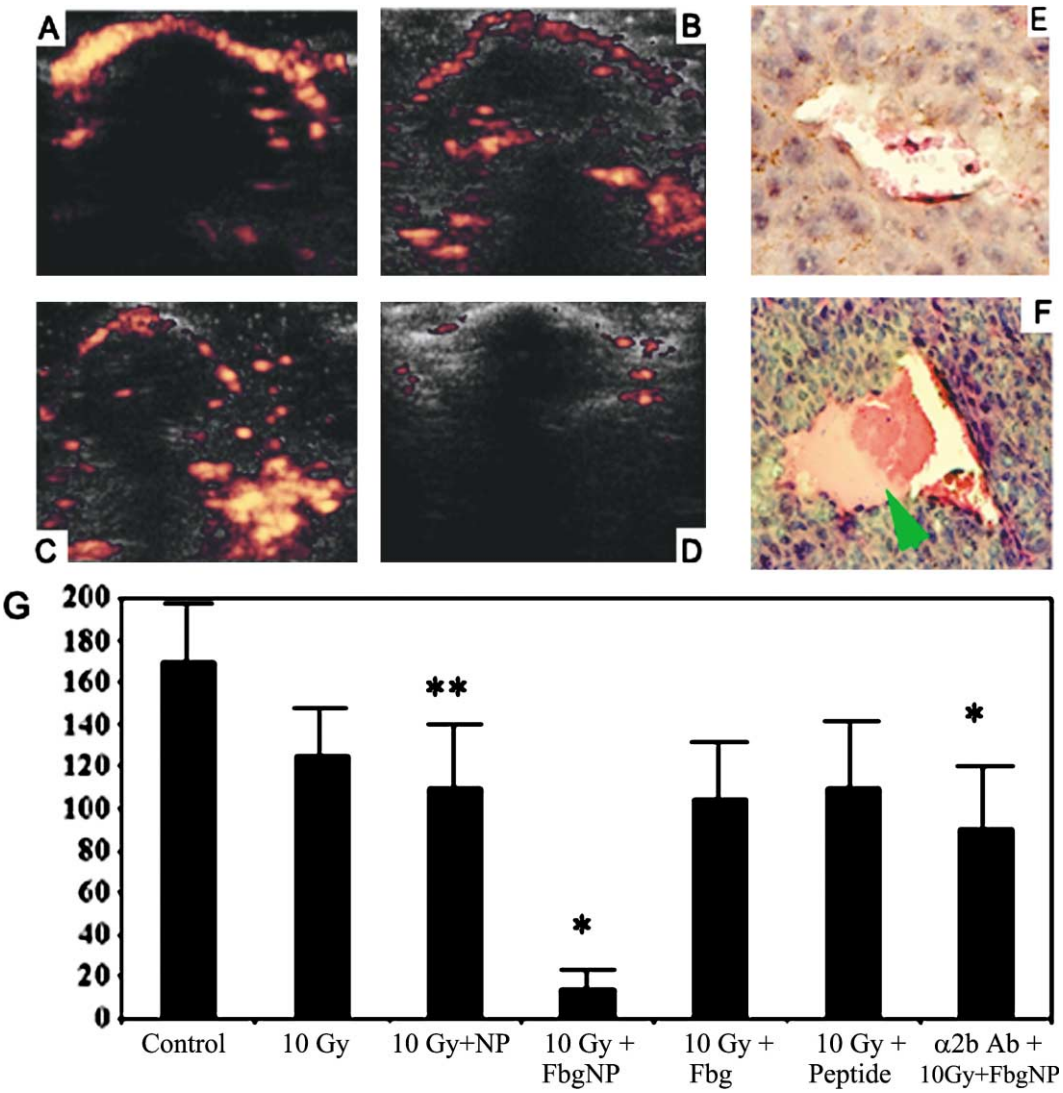

Figure 6. Tumor blood flow analysis by use of ampulate modulated Doppler ultrasound

B16F0 hind limb tumors were imaged by Power Doppler sonography. Color area was recorded for the entire tumor. Shown are representative color sonographic images of (**A**) 0 Gy, (**B**) 10 Gy alone, (**C**) 10 Gy and uncoated nanoparticles, or (**D**) 10 Gy and Fbg-NP. Increased signal intensity indicates areas of high blood flow. Absence of signal indicates minimal blood flow.

E and **F**: Thrombus formation within tumors treated with Fbg-NP and radiation. Tumors shown in **D** were sectioned and stained with H&E. Shown are microscopic photographs of tumors treated with 6 Gy and (**E**) uncoated nanoparticles, or (**F**) Fbg-NP. Arrow indicates thrombus formation within a treated tumor blood vessel.

G: The bar graph shows the mean and SEM of power-weighted pixel density (PWPD) in ten mice entered into each treatment group. Signal intensity (color) was quantified using HDI-lab software. Blood flow was measured in tumors at 0 hr and 72 hr after treatment with 0 Gy, 10 Gy alone, 10 Gy and uncoated nanoparticles (NP), 10 Gy and Fbg-NP (Fbg-NP), fibrinogen and 10 Gy, HHLGGAKQAGDV peptide and 10 Gy, or α2b blocking antibody injected prior to Fbg-NP and irradiation. The percent change in tumor blood flow is shown. Values for color area were averaged for each of the treated groups and are compared to the same tumor prior to treatment by use of unpaired Student's t test (**p = 0.023; *p = 0.048).

NP alone achieved no tumor regression and no significant growth delay as compared to untreated control tumors. Radiation alone achieved minimal growth delay as compared to untreated control tumors ($p = 0.11$). Uncoated albumin nanoparticles served as a negative control. When administered with irradiation, albumin nanoparticles produced tumor growth rate that was identical to that of tumors treated with radiation alone. Fbg-NP administered with irradiation resulted in tumor regression and a significant growth delay as compared to tumors treated with uncoated albumin nanoparticles and irradiation ($p = 0.024$).

Discussion

Radiation-induced physiologic changes in tumor blood vessels include conformational changes in pre-existing receptors or transport of sequestered proteins (Hallahan et al., 1998). These candidates for drug delivery cannot be detected by analysis of differential expression because protein and mRNA levels will not change. Therefore, we utilized phage displayed peptide libraries, which are useful discovery tools for the identification of tumor-specific receptors in animal models (Arap et al., 1998).

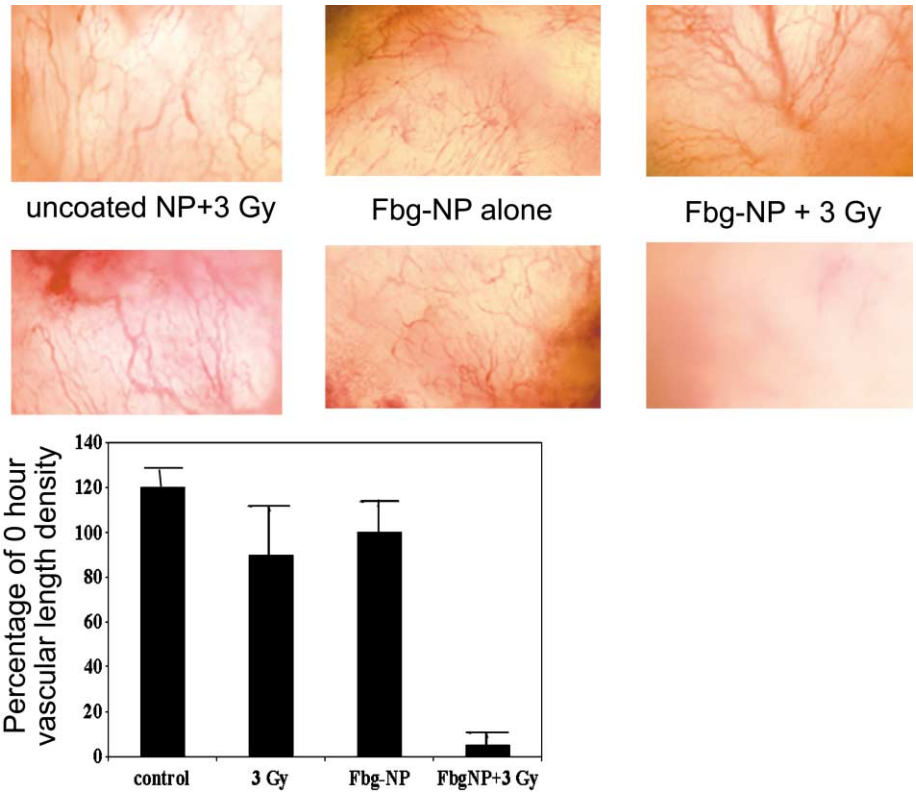

Figure 7. Tumor vascular windows showing absence on hemoglobin within treated tumor blood vessels

LLC tumors were implanted into the dorsal skin fold window of C57BL6 mice. Shown are representative microscopic photographs of tumor vascular windows before (0 hr) and after (72 hr) treatment with uncoated nanoparticles and radiation alone, Fbg-NP alone, or combined Fbg-NP and radiation. The bar graph shows the mean and SEM of five tumors in each of these treatment groups.

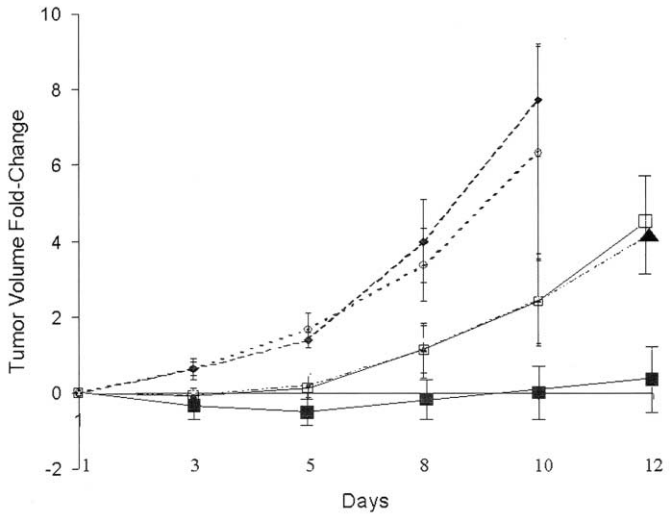

Figure 8. Fold increase in mean tumor volume

B16F0 tumors implanted into the hind limb of C57BL6 mice were treated with 10 Gy with or without the indicated nanoparticles. Tumor volumes were measured on the indicated days by use of calipers. Ten mice were entered into each of five groups (untreated control ◇, radiation alone ð, Fbg-NP alone O, Fbg-NP + radiation □, and albumin nanoparticles + radiation Δ). Uncoated albumin nanoparticles served as a negative control. Fbg-NP administered with irradiation resulted in tumor regression and a significant growth delay as compared to tumors treated with uncoated albumin nanoparticles and irradiation ($p = 0.024$, Kruskal-Wallis).

In the present study, the peptide library was injected into the venous circulation and adhered to receptors in irradiated tumor blood vessels. These phage peptides were then repeatedly recovered from irradiated tumors through several passages. Peptides that bind nonspecifically to untreated blood vessels will bind within other organs. The amino acid sequence RGDGSSV was recovered from multiple tumor models and binds within the tumor vascular lumen following irradiation. The $\alpha 2b\beta 3$ integrin on platelets and the $\alpha v\beta 3$ integrin on endothelium play an important role in angiogenesis (Reynolds et al., 2002; Trikha et al., 2002; Silletti et al., 2001), and bind the RGD peptide sequence within tumor microvasculature (Hood et al., 2002; Maeshima et al., 2001). We studied selective ligands to $\alpha v\beta 3$ to determine whether this is the binding site for the recovered phage peptide RGDGSSV. There was no increase in the staining for the αv chain of integrin $\alpha v\beta 3$ in irradiated tumor vessels. Moreover, we found no increased binding of $\alpha v\beta 3$ ligands to tumor blood vessels following irradiation (D.H., unpublished data). To determine the specificity of Fbg-NP binding, we utilized $\alpha 2b$- and αv-blocking antibodies to compete for radiation-induced ligand binding. This showed that the $\alpha 2b$ antibody prevented targeting of ligand, while the αv-blocking antibody had no effect on ligand binding. Taken together with the findings that $\alpha 2b\beta 3$ accumulates in irradiated tumor blood vessels, the fibrinogen receptor was selected for radiation-guided drug delivery.

Fbg-NP and liposomes bind selectively within irradiated tumor blood vessels. We found little to no binding in other organs. Platelets are activated during normal physiologic conditions such as during wound repair. We have found that Fbg-NP bind

to sites of mechanical injury (D.H., unpublished data). However, there were no thrombotic emboli to organs such as the brain, lung, kidney, or liver. The spleen acts as a trap during the removal of activated platelets and Fbg-NP from the circulation. Moreover, the mice do not develop tachypnea or hypomotility following Fbg-NP injection and irradiation. Future phase I trials could demonstrate the need to administer nanoparticle by an intra-arterial approach; however, ongoing clinical trials have not shown a risk of thrombotic events. A clinical trial designed to test the feasibility of targeting drug delivery to radiation-activated integrins is underway. This clinical study utilizes the peptidomimetic designed to evaluate deep venous thrombosis by binding to activated α2bβ3 (Hallahan et al., 2001). Biapcitide (Acutect, Diatide/Berlex) is a structural analog of the RGD peptide. Biapcitide is labeled with ^{99}Tc and administered to patients receiving stereotactic radiosurgery or high dose rate brachytherapy. Our preliminary data show that biapcitide binds to irradiated tumors and that ^{99}Tc is selectively localized by use of irradiation.

Ionizing radiation induces the expression of antigens in the vascular endothelium through posttranslational modification and transcriptional induction of cell adhesion molecules and integrins (Hallahan et al., 1995b, 1996 1998; Hallahan and Virudachalam, 1999). X-ray-induced activation of integrin $\alpha_{2b}\beta_3$ is one potential radiation-inducible molecular target that can be exploited for drug delivery to tumor microvasculature. Radiation is localized to the tumor through the use of conformal irradiation, intensity-modulated radiotherapy, brachytherapy, and stereotactic irradiation. The threshold dose for antigen induction can be exceeded in the neoplasm, but avoided in the surrounding normal tissues. Ionizing radiation increases tumor vascular permeability (Yu et al., 2002). In the present study, uncoated nanoparticles and liposomes were used as controls to determine whether tumor targeting was in part due to increased tumor vascular permeability. Uncoated control nanoparticles and liposomes showed no increase in tumor localization following irradiation.

Tumor-specific drug delivery has the potential to minimize toxicity to normal tissues and improve bioavailability of cytotoxic agents to neoplasms (Arap et al., 1998; Kasahara et al., 1994). Existing site-specific drug delivery systems include adenovirus-targeted delivery to endothelial receptor $\alpha_v\beta_3$ (Brooks et al., 1994; Wickham et al., 1995), and tumor-specific antigens (Ito et al., 1991; Manome et al., 1994). Antibody conjugation to cytotoxic agents has shown promise in achieving the goal of tumor-targeted cytotoxicity (Hellstrom et al., 1996; Pastan, 1997). Liposome conjugation to proteins has also been used to deliver chemotherapy such as Doxorubicin to tumor-specific antigens (Kirpotin, 1997). Each of these targeting approaches has been limited by nonspecific binding to normal tissues or limited to very specific subsets of neoplasms, and by the small subsets of tumors that can be targeted by these antibodies, and by poor biodistribution of antibodies into solid tumors (Jain, 1997). Alternative approaches to target all neoplasms exploit integrins and antigens on proliferating microvasculature (Burg et al., 1999; Pasqualini and Ruoslahti, 1996). Radiation-inducible antigens include proteins in the microvasculature of irradiated tumors, which are antigenic targets for site-specific drug delivery to tumor blood vessels. The advantage in radiation targeting of drug delivery is that the physiologic response of vasculature to radiation is similar among all tumors studied in this investigation. In addition to GL261, B16F0, and LLC, we also studied ligand binding within irradiated H460 human tumor xenografts in nude mice, which showed site-specific drug delivery and obliteration of tumor blood flow in a human xenograft.

The microvasculature is a therapeutic target in the treatment of cancer. One endothelial cell supplies nutrients to many tumor cells. Tumor vasculature is therefore an effective therapeutic target in treatment of neoplasms (Folkman, 1995). Thrombotic destruction of blood flow can achieve ischemia and subsequent tumor necrosis. Tumor vascular embolization is a strategy to achieve obliteration of tumor blood flow. Platelet aggregation begins immediately after irradiation and accumulates over 6 hr, when maximal platelet aggregation is achieved. In the present study, Fbg-NP administered concurrently with irradiation resulted in significant reduction in tumor blood flow and subsequent tumor growth delay as compared to tumors treated with uncoated albumin nanoparticles and irradiation. Fbg-NP can accumulate by binding to the fibrinogen receptor on these activated platelets. The risk of thromboembolic events resulting from fibrinogen-conjugated nanoparticles warrants further development of targeted drug delivery to radiation-activated α2bβ3 integrin.

Experimental procedures

Recombinant T7 bacteriophage

The T7 phage display system has the capacity to display peptides up to 15 amino acids in size at the high copy number (415 per phage). Unlike the filamentous systems, peptides displayed on the surface of T7 are not capable of secretion to the cell membrane as required for the filamentous phage assembly. T7 also replicates more rapidly and is extremely robust as compared to other phage. The stability allows for bio-panning selection procedures, which require that phage remain infective. The T7 phage display system exploits the T7 capsid protein to display peptides on the surface of phage. The capsid gene 10 encodes a protein that is 348 amino acids in length that can accommodate variation. The region of the capsid protein unique to the 10B protein is on the surface of the phage and can be used for phage display. Gene 10 encoding the capsid protein is cloned with a series of multiple cloning sites at the C terminus of the 10B protein. The natural translational frameshift site within the capsid gene has been removed so that only a single form of the capsid protein is made. This results in a total of 415 recombinant peptides expressed on the surface of the phage.

We utilized the recombinant bacteriophage library in T7 phage (Novagen). A population of DNA fragments encoding our recombinant peptide sequences was cloned into the T7 select vector, packaged into phage, and amplified to prepare the library for bio-panning in the lab of E. Ruoslahti. The ecoR1 estrogen enzyme site was selected to insert our random sequence of DNA segments. This allowed for directional cloning of prepared DNA inserts and expression in-frame with the 10B protein such that the recombinant fusion proteins were displayed. The resulting reading frame requires the AAT (Asn) initial codon followed by a TCX (Ser) codon. Size-fractionated cDNA inserts were prepared by gel filtration on sepharose 4B and ranged from 27 to 33 nucleotides. cDNAs were ligated by use of the DNA ligation kit (Novagen). The recombinant T7 DNA was then packaged in the packaging extract provided by Novagen. The packaged recombinant phage display library was then amplified prior to beginning the bio-panning in animal tumor models (Condron et al., 1991; Russel, 1991).

Our goal was to discover peptides that bind within the vascular endothelium of all irradiated tumors. We therefore utilized two distinct tumor models including GL261 gliomas and B16F0 melanoma implanted into C57BL6 mice. Tumors were implanted into the hind limb of mice. Tumors were then irradiated with 3 Gy. The entire phage library was administered by intracardiac injection at 4 hr following irradiation. The mouse was then perfused with 10 ml of PBS into the left ventricle that was recovered from the right atrium. Five minutes following irradiation, tumors were resected and phage were recovered from tumor homogenates. Tissue was disrupted by use of hand-held homogenizer on ice. Recovered phage were then amplified 10^6-fold by use of BL21 bacteria and subsequently administered to a second round of

irradiated tumors at 4 hr following treatment. Once again, tumors were resected and phage were recovered and amplified. This sequence was repeated six times before sequencing of the capside DNA within the recovered phage. Following recovery from six sequential irradiated tumors, the phage were plated in bacterial culture in auger. Lytic sites within the bacterial culture were isolated and amplified. The DNA from 50 phage colonies was sequenced.

PCR was used to amplify the recombinant phage insert coding region directly from the plaques. We sequenced 50 clones following six rounds of selection. We identified sequences that appear multiple times after six rounds of bio-panning. The PCR primer pair includes a T7 "up" primer, a 20-mer with the sequence AGC GGA CCA GAT TAT CGC TA (Novagen). The T7 "down" primer is a 20-mer with the sequence AACCCTCAAGACCCGTTTA. The primer pair solution was prepared in 0.2 pmol/ul in water. The PCR beads were dissolved in 24 μl of primer pair solution. The T7 plaque was suspended in 10 μl of 1× tris-buffered saline. The PCR reaction mixture was mixed with 1 μl of phage suspension. The sequencing reaction was performed as described and separated by sequencing gel in an ABI 377 sequencer.

Intravital tumor vascular window model

Gibco BRL penicillin-streptomycin solution (200 μl) was injected into the hind limb of the mouse before the procedure. The dorsal skin fold window is a 3 g plastic frame applied to the skin of the mouse and remains attached for the duration of the study. The chamber was screwed together, while the epidermis was incised and remained open with a plastic covering. During surgery, the area was kept moist by applying moist drops of phosphate-buffered saline with 1% Penicillin/Streptomycin Solution. The bottom portion of the chamber was put in place and the top was carefully positioned on the cut side so that the window and the circular incision were fitted. Antibiotic ointment was applied at this time. Tumor blood vessels developed in the window within 1 week. Vascular windows were treated with 6 Gy using superficial X-rays using 80kVp. FITC-labeled peptide (Genemed Synthesis, Inc., South San Francisco, California) was administered by tail vein immediately prior to irradiation. Vascular windows were photographed using fluorescence microscopy and 4× objective to obtain a 40× total magnification. Binding of FITC-labeled peptide was photographed at 6 hr after irradiation.

Immunohistochemistry of tumor sections

GL261 murine gliomas were implanted into the hind limb of C57BL6 mice. Tumors were grown to a diameter of 10–12 mm over 8–10 days. Tumors were irradiated with 10 Gy and fixed 6 hr later. Immunohistochemical staining for P-selectin and integrin $\alpha_{2b}\beta_3$was performed for untreated control and tumors 6 hr after irradiation. Sections were stained with rabbit anti-mouse α_{2b} or β3 antibodies (CD41/61; BD Sciences), and HRP-conjugated goat anti-rabbit IgG (Vector Labs, Burlingame, California) as described (Hallahan and Virudachalam, 1999; Hallahan et al., 1998).

Microsphere preparation

Albumin nanoparticles (Martodam et al., 1979) were resuspended using 10 ml of sterile normal saline (0.9% NaCl). One half milliliter of the reconstituted microsphere was added to a 1.5 ml conical polypropylene tube previously coated with Iodgen (Pierce, Rockford, Illinois). To this, 11.3 mCi (418 megabecquerel (MBq)) of ^{131}I-Dupont (North Billerica, Massachusetts) NEZ-035H was added in approximately 11 μl of saline and allowed to incubate at room temperature for 30 min. Following incubation, the nanoparticles were transferred to a 15 ml sterile centrifuge tube, diluted to 10 ml with normal saline, and centrifuged at 1,500 × "gravity" for 7 min. The supernatant was removed and discarded. The nanoparticles were washed one additional time with 10 ml of normal saline and centrifuged. The nanoparticles were suspended in 2 ml of normal saline for injection. Final yield was 4.8 mCi (177.6 MBq) of radioiodinated nanoparticles in 2 ml saline. Radiochemical yield was 42.4%. Nanoparticles were radiolabeled, and the radioiodination process was terminated by removing the reaction mixture from the reaction vessel into a centrifugation tube. The reaction mixture was centrifuged at 3000 rpm for 15 min. The supernatant were removed and the residue was reconstituted in 5 ml sterile normal saline.

Preparation and radioiodination of proteins

Twenty milliliter glass scintillation vials were depyrogenized and sterilized by rising them in deionized water followed by putting them into an oven at 150°C overnight. Iodogen iodination solution was prepared by dissolving 1 mg iodogen in every 10 ml of chloroform. Ten milliliters of the prepared iodogen iodination reagent solution was then added to each depyrogenized 20 ml glass scintillation vial. The solvent was slowly evaporated off by gently passing a stream of dry filtered nitrogen over it. When all the solvent had been evaporated, a fine white film of iodogen was evenly plated on the inner wall of the vessel. The vessels were sealed and placed in a desicator until use.

Each vial of peptides to be radioiodinated was stored at 0°C–4°C and was reconstituted immediately prior to radioiodination with 5 ml of sterile normal saline. The iodogen-plated reaction vessel was rinsed with a small amount of sterile saline to remove any loose microscopic flakes of the iodination reagent. The desired amount of carrier-free I-125 sodium iodide were added to the reaction vessel, followed by the reconstituted peptides suspension. We used a specific activity of 100 μCi/μg protein. The reaction vessel was sealed off and the reaction was allowed to proceed for 20 min at room temperature with constant gentle agitation of the reaction vessel. Radiolabeled protein was isolated by gel chromatography.

GL261 murine gliomas and B16F0 murine melanomas were implanted into the hind limb of C57BL6 mice. ^{131}I-nanoparticles were administered by tail vein injection and mice were imaged by pinhole collimator on an Anger γ camera.

Animal imaging and image analysis

Tumor bearing mice were imaged at 1 hr and 24 hr time points post-administration of radiolabeled proteins. Planar pinhole γ camera imaging was performed on a single-head γ camera (General Electric Helix®) using a cone-shaped pinhole collimator with a 4 mm diameter Tungsten aperture. Pinhole collimation offers the advantage of improved photon detection efficiency (sensitivity) and spatial resolution when compared with conventional, parallel multihole collimators. Pinhole planar imaging with a small source-aperture separation can provide high-resolution images combined with large magnification. Each scan consisted of a 180 s acquisition (256 × 256 acquisition matrix) with a 10% energy window centered on 364keV. The source-aperture separation was 6.0 cm. Prior to the animal studies, a uniform ^{131}I disk source was imaged in order to measure the angular dependence of the pinhole collimator to gamma camera system detection efficiency with distance from the center of the pinhole. Angular sensitivity, normalized to 1.0 at the center of the pinhole, was then used to scale the mouse data in order to correct image counts for this geometrical effect. A calibration source of known ^{131}I activity was also scanned at a 6.0 cm source-aperture separation distance in order to measure system sensitivity along the center of the pinhole.

Fibrinogen conjugation to liposome

The lipophilic SH reactive reagent with a long spacing arm was synthesized from malimide-PGE 2000-NSH ester (Prochem), dioleoylphosphatidylethanolanime (DOPE, Avanti Polar Lipids), and triethylamine in chloroform (1:1:1.5). Resulting maleimide-PEG 2000-DOPE was purified by flash column. Under stirring, 5× excess of freshly prepared Traut's reagent in the same buffer was added to a solution of fibrinogen (2 mg/ml) in 0.01 M HEPES 0.15 NaC1 buffer (pH 7.9), containing 10 mM EDTA and 0.08% NaN_3. Reaction was performed for 30 min at 0°C. SH-fibrinogen was then purified using a desalting PD-10 column. PGE 2000-PE, cholesterol, Dipalmitoyl phosphocholine (Avanti Polar Lips, AL), DiI (lipid fluorescent marker), and maleimide-PEG-2000-DOPE were dissolved in chloroform and mixed at a molar ratio of 10:43:43:2:2 in a round bottom flask. The organic solvent was removed by evaporation followed by desiccation under vacuum for 2 hr. Liposomes were prepared by hydrating the dried lipid film in PBS at a lipid concentration of 10 mM. The suspension was then sonicated 3 × 5 min until clear, forming unilamellar liposomes of 100 nM in diameter. To conjugate thiolated fibrinogen to maleimide containing liposomes, prepared vesicles and thiolated protein were mixed in 10 mm Hepes, 0.15M NaC1, and EDTA (pH 6.5). The final concentrations for proteins and liposomes were 0.25 g/l and 2.5 mM, respectively. Mixture was incubated for 18 hr at RT and vesicles were separated from unconjugated protein by gel filtration (sepharose 4B-CL, Pharmacia).

Liposomes were fluorescently labeled with DiI fluorescent marker and administered by tail vein to tumor bearing mice. Tumors were treated with 4 Gy either prior to administration or after administration of fibrinogen-

liposome conjugates. Tumors were fixed and sectioned at 24 hr following irradiation. Fluorescence was imaged by UV microscopy (100×).

Analysis of tumor blood flow

C57BL/6 mice injected subcutaneously in the right hind limb with 10^6 viable cells of a murine glioblastoma (GL261) suspended in 0.2 ml of a 0.6% solution of agarose. Each set of ten mice was stratified into four groups on day 1 (radiation, nanoparticles, nanoparticles + radiation, untreated control, HHLGGAKQAGDV peptide and radiation, and fibrinogen (Sigma) and radiation). Mouse tumors were stratified into groups so that the mean tumor volume of each group was comparable. Irradiated mice were immobilized in Lucite chambers and the entire body was shielded with lead except for the tumor-bearing hind limb. Tumors were treated with 6 Gy superficial X-rays using 80kVp (Pantak X-ray Generator).

Blood flow within these tumors was quantified by Power Doppler after the third fraction of irradiation. Tumor blood flow was imaged with a 10–5 MHz linear Entos® probe attached to an HDI 5000 (probe and HDI 5000 from ATL/Philips, Bothell, Washington) as we have previously described (Donnelly et al., 2001; Geng et al., 2001). Power Doppler sonography images were obtained with the power gain set to 82%. A 20 frame cineloop sweep of the entire tumor was obtained with the probe perpendicular to the long axis of the lower extremity along the entire length of the tumor. Color area was quantified using HDI-lab software (ATL/Philips, Bothell, Washington). This software allows direct evaluation of power Doppler cineloop raw. Color area was recorded for the entire tumor. Five mice were entered into each treatment group. Values for color area were averaged for each tumor set and treated groups were compared to controls with the unpaired Student's t test.

Tumor growth delay

C57BL/6 mice injected subcutaneously in the right thigh with 10^6 viable cells of a murine B16F0 melanoma suspended in 0.2 ml of a 0.6% solution of agarose. Each set of ten mice was stratified into five groups (untreated control, radiation alone, Fbg-NP alone, Fbg-NP + radiation, and albumin nanoparticles + radiation) to control for mean tumor volume. An equal number of large and intermediate size tumors were present in each group. Mouse tumors were stratified into groups so that the mean tumor volume of each group was comparable. Irradiated mice were immobilized in Lucite chambers and the entire body was shielded with lead except for the tumor-bearing hind limb.

Twice weekly tumor volumes were measured using skin calipers as previously described (Geng et al., 2001). Tumor volumes were calculated from a formula ($a \times b \times c/2$) that was derived from the formula for an ellipsoid ($\pi d^3/6$). Data were calculated as the fold increase of original (day 1) tumor volume and graphed as fold increase tumor volume ± 95% confidence intervals for each treatment group, and variance was analyzed by the Kruskal-Wallis (Kruskal and Wallis, 1952). Fibrinogen-coated albumin nanoparticles were prepared as described above and administered by tail vein injection immediately prior to irradiation. Uncoated albumin nanoparticles served as a negative control. Tumors were irradiated with a single dose of 10 Gy by use of 80kVp X-ray generator.

Acknowledgments

We thank Errki Ruoslahti for peptide phage libraries and Ali Fu, Robert C. Iverson, George Holburn, James Patton, Dawn Shone, Helina Onishko, and Jason Dugger for their technical assistance. This work was supported by NIH grants (R21-CA89888, R01-CA70937, R01-CA58508, P30-CA68485, R01-CA88076, R01-CA89674, and the Vanderbilt Lung Cancer SPORE P50-CA90949), by a training grant from American Society Therapeutic Radiology Oncology, and by developmental funds from the Vanderbilt Department of Radiation Oncology.

Received: May 16, 2002
Revised: December 9, 2002

References

Arap, W., Pasqualini, R., and Ruoslahti, E. (1998). Cancer treatment by targeted drug delivery to tumor vasculature in a mouse model. Science *279*, 377–380.

Baillie, C., Winslet, M., and Bradley, N. (1995). Tumour vasculature—a potential therapeutic target. Br. J. Cancer *72*, 257–267.

Boerman, O., Rennen, H., Oyen, W., and Corstens, F.H. (2001). Radiopharmaceuticals to image infection and inflammation. Semin. Nucl. Med. *31*, 286–295.

Brooks, P.C., Montgomery, A.M., Rosenfeld, M., Reisfeld, R.A., Hu, T., Klier, G., and Cheresh, D.A. (1994). Integrin alpha v beta 3 antagonists promote tumor regression by inducing apoptosis of angiogenic blood vessels. Cell *79*, 1157–1164.

Burg, M., Pasqualini, R., Ruoslahti, E., and Stallcup, W. (1999). NG2 proteoglycan-binding peptides target tumor neovasculature. Cancer Res. *59*, 2869–2874.

Condron, B.G., Atkins, J.F., and Gesteland, R.F. (1991). Frameshifting in gene 10 of bacteriophage T7. J. Bacteriol. *173*, 6998–7003.

Donnelly, E., Fleischer, A., Thirsk, M., and Hallahan, D. (2001). Sonographic quantification of changes in tumor vascularity after radiation and/or chemotherapy in an animal model. Radiology *219*, 166–170.

Dvorak, H.F., Nagy, J.A., and Dvorak, A.M. (1991). Structure of solid tumors and their vasculature: implications for therapy with monoclonal antibodies. Cancer Cells *3*, 77–85.

Ellerby, H.M., Arap, W., Ellerby, L.M., Kain, R., Andrusiak, R., Rio, G.D., Krajewski, S., Lombardo, C.R., Rao, R., Ruoslahti, E., et al. (1999). Anticancer activity of targeted pro-apoptotic peptides. Nat. Med. *5*, 1032–1038.

Folkman, J. (1995). Seminars in medicine of the Beth Israel Hospital, Boston. Clinical applications of research on angiogenesis. N. Engl. J. Med. *333*, 1757–1763.

Forrer, P., Jung, S., and Pluckthun, A. (1999). Beyond binding: using phage display to select for structure, folding and enzymatic activity in proteins. Curr. Opin. Struct. Biol. *9*, 514–520.

Fox, S., and Harris, A.L. (1997). Markers of tumor angiogenesis: clinical applications in prognosis and anti-angiogenic therapy. Invest. New Drugs *15*, 15–28.

Geng, L., Donnelly, E., Lin, C., Sierra-Rivera, E., Onishko, H., and Hallahan, D. (2001). Inhibiton of VEGF receptor reverses the resistant phenotype. Cancer Res. *61*, 2413–2419.

Hallahan, D.E., and Virudachalam, S. (1999). CD62P (P-selectin) translocation to the vascular lumen in blood vessels exposed to ionizing radiation. Radiat. Res. *152*, 6–13.

Hallahan, D.E., Clark, E.T., Kuchibhotla, J., Gewertz, B., and Collins, T. (1995a). E-selectin gene induction by ionizing radiation is independent of cytokine induction. Biochem. Biophys. Res. Commun. *217*, 784–795.

Hallahan, D.E., Mauceri, H.J., Seung, L.P., Dunphy, E.J., Toledano, A., Hellman, S., Kufe, D.W., and Weichselbaum, R.R. (1995b). Spatial and temporal control of gene therapy by ionizing radiation. Nat. Med. *1*, 786–791.

Hallahan, D.E., Kuchibholta, J., and Wyble, C. (1996). Cell adhesion molecules mediate radiation-induced leukocyte adhesion to the vascular endothelium. Cancer Res. *56*, 5150–5155.

Hallahan, D.E., Virudachalam, S., Kolchinsky, A., and Staba, M.J. (1998). X-ray induced expression of P-selectin in tumor blood vessels. Cancer Res. *58*, 5216–5220.

Hallahan, D., Chen, A., Teng, M., Cmelak, A., and Staba, M.J. (1999). Drug-radiation interactions in tumor blood vessels. Oncology *13*, 71–77.

Hallahan, D.E., Geng, L., Cmelak, A., Chakravarthy, A.B., Scarfone, C., and Gonzalez, A. (2001). Targeting drug delivery to radiation-induced neoantigens in tumor microvasculature. J. Control. Release *74*, 183–191.

Hellstrom, I., Trail, P., Siegall, C., Firestone, R., and Hellstrom, K. (1996).

Immunoconjugates and immunotoxins for therapy of solid tumors. Cancer Chemother. Pharmacol. *38*, 35–36.

Hood, J.D., Bednarski, M., Frausto, R., Guccione, S., Reisfeld, R.A., Xiang, R., and Cheresh, D.A. (2002). Tumor regression by targeted gene delivery to the neovasculature. Science *296*, 2404–2407.

Ito, T., Griffin, T.W., Deng, H., Collins, J.A., Bril, A.B., and Johnson, D.K. (1991). Preclinical assessment of 90Y-labels C110 anti-CEA immunotoxin: a potent therapeutic immunoconjugate for human colon cancer. Cancer Res. *51*, 255–260.

Jain, R.K. (1997). The Eugene M. Landis Award Lecture 1996. Delivery of molecular and cellular medicine to solid tumors. Microcirculation *4*, 1–23.

Kasahara, N., Dozy, A., and Kan, Y. (1994). Tissue-specific targeting of retroviral vectors through ligand-receptor interactions. Science *266*, 1373–1376.

Kirpotin, D. (1997). Sterically stabilized anti-HER2 immunoliposomes: design and targeting to human breast cancer cells in vitro. Biochemistry *7*, 66–75.

Kruskal, W.H., and Wallis, W.A. (1952). Use of ranks in one-criteria variance analysis. J. Am. Stat. Assoc. *47*, 583–621.

Llovet, J.M., Real, M.I., Montana, X., Planas, R., Coll, S., Aponte, J., Ayuso, C., Sala, M., Muchart, J., Sola, R., et al. (2002). Arterial embolisation or chemoembolisation versus symptomatic treatment in patients with unresectable hepatocellular carcinoma: a randomised controlled trial. Lancet *395*, 1734–1739.

Maeshima, Y., Yerramalla, U.L., Dhanabal, M., Holthaus, K.A., Barbashov, S., Kharbanda, S., Reimer, C., Manfredi, M., Dickerson, W.M., and Kalluri, R. (2001). Extracellular matrix-derived peptide binds to alpha(v) beta(3) integrin and inhibits angiogenesis. J. Biol. Chem. *276*, 31959–31968.

Manome, Y., Abe, M., Hagen, M., Fine, H., and Kufe, D. (1994). Enhancer sequences of the DF3 gene regulate expression of the herpes simplex virus thymidine kinase gene. Cancer Res. *54*, 5408–5413.

Martodam, R.R., Twumasi, D.Y., Liener, I.E., Powers, J.C., Nishino, N., and Krejcarek, G. (1979). Albumin microspheres as carrier of an inhibitor of leukocyte elastase: potential therapeutic agent for emphysema. Proc. Natl. Acad. Sci. USA *76*, 2128–2132.

McGinity, J.W., and O'Donnell, P.B. (1997). Preparation of nanospheres by the solvent evaporation technique. Adv. Drug Deliv. Rev. *13*, 25–42.

Molema, G., de Leij, L., and Meijer, D. (1997). Tumor vascular endothelium: barrier or target in tumor directed drug delivery and immunotherapy. Pharm. Res. *14*, 2–10.

Pasqualini, R., and Ruoslahti, E. (1996). Organ targeting in vivo using phage display peptide libraries. Nature *380*, 364–366.

Pastan, I. (1997). Targeted therapy of cancer with recombinant immunotoxins. Biochim. Biophys. Acta *1333*, 1–6.

Rajotte, D., and Ruoslahti, E. (1999). Membrane dipeptidase is the receptor for a lung-targeting peptide identified by *in vivo* phage display. J. Biol. Chem. *274*, 11593–11598.

Reynolds, L.E., Wyder, L., Lively, J.C., Taverna, D., Robinson, S.D., Huang, X., Sheppard, D., Hynes, R.O., and Hodivala-Dilke, K.M. (2002). Enhanced pathological angiogenesis in mice lacking beta3 integrin or beta3 and beta5 integrins. Nat. Med. *8*, 27–34.

Ruoslahti, E. (1996). RGD and other recognition sequences for integrins. Annu. Rev. Cell Dev. Biol. *12*, 697–715.

Russel, M. (1991). Filamentous phage assembly. Mol. Microbiol. *5*, 1607–1613.

Saltzman, W.M., and Fung, L.K. (1997). Polymeric implants for cancer chemotherapy. Adv. Drug Deliv. Rev. *26*, 209–230.

Santoro, S.A., and Lawing, W.J., Jr. (1987). Competition for related but nonidentical binding sites on the glycoprotein IIb-IIIa complex by peptides derived from platelet adhesive proteins. Cell *48*, 867–873.

Shockley, T.R., Lin, K., Nagy, J.A., Tompkins, R.G., Dvorak, H.F., and Yarmush, M.L. (1991). Penetration of tumor tissue by antibodies and other immunoproteins. Ann. N Y Acad. Sci. *618*, 367–382.

Silletti, S., Kessler, T., Goldberg, J., Boger, D.L., and Cheresh, D.A. (2001). Disruption of matrix metalloproteinase 2 binding to integrin alpha v beta 3 by an organic molecule inhibits angiogenesis and tumor growth in vivo. Proc. Natl. Acad. Sci. USA *98*, 119–124.

Sipkins, D., Gijbels, K., Tropper, F., Bednarski, M., Li, K., and Steinman, L. (2000). ICAM-1 expression in autoimmune encephalitis visualized using magnetic resonance imaging. J. Neuroimmunol. *104*, 1–9.

Smith, J.W., and Cheresh, D.A. (1988). The arg-gly-asp binding domain of the vitronectin receptor: photoaffinity crosslinking implicates amino acid residues 61–203 of the β subunit. J. Biol. Chem. *263*, 18726–18731.

Trikha, M., Zhou, Z., Timar, J., Raso, E., Kennel, M., Emmell, E., and Nakada, M.T. (2002). Multiple roles for platelet GPIIb/IIIa and alpha v beta3 integrins in tumor growth, angiogenesis, and metastasis. Cancer Res. *62*, 2824–2833.

Wickham, T., Carrion, M.E., and Kovesdi, I. (1995). Targeting of adenovirus penton base to new receptors through replacement of its RGD motif with other receptor-specific peptide motifs. Gene Ther. *2*, 750–756.

Yu, H., Su, M.Y., Wang, Z., and Nalcioglu, O. (2002). A longitudinal study of radiation-induced changes in tumor vasculature by contrast-enhanced magnetic resonance imaging. Radiat. Res. *158*, 152–158.

Zwick, M.B., Shen, J., and Scott, J.K. (1998). Phage-displayed peptide libraries. Curr. Opin. Biotechnol. *9*, 427–436.